Equilibrium solute segregation to matrix-θ' precipitate interfaces in Al-Cu alloys from first principles

G. D. Samolyuk,[1,*] M. Eisenbach,[1] D. Shin,[1] Y. N. Osetsky,[1] A. Shyam,[1] and J. R. Morris[2,†]
[1]*Oak Ridge National Laboratory, Oak Ridge, Tennessee 37831, USA*
[2]*Ames Laboratory, Ames, Iowa 50011, USA*

(Received 9 October 2019; accepted 1 June 2020; published 6 July 2020)

Particular combinations of solute atoms segregated to the interface of the Al and θ'-Al_2Cu in Al-Cu alloys can help stabilize θ' precipitates at high temperatures. Stabilization of such precipitates is determined by a combination of thermodynamics (including driving forces for coarsening and transformation and solute segregation tendencies) and kinetic effects (including solute diffusion and interfacial mobility in the presence of interfacial solute segregation). For some alloys such as recent Al-Cu-based alloys, multiple solutes segregate in significant quantities to interfaces, and solute-solute interactions at the interface are important, with multiple types of solutes competing for similar interfacial sites. To treat this situation, we develop and apply a statistical mechanics approach to calculate the temperature-dependent equilibrium solute atoms distribution near the coherent and semicoherent interfaces between the Al matrix and the θ'-Al_2Cu precipitates. The developed approach is applied to the investigation of Si, Mn, and Zr segregation at the interface, as particular combinations of these elements affect the thermal stability of the θ' precipitates. We demonstrate that because Si and Mn atoms segregate on the same semicoherent interface, the presence of Si reduces the concentration of Mn solutes at the interface. Si atoms preferably occupy the first layer of the interface and compete with Mn atoms for one type of particular sites in the layer. Mn atoms preferably occupy the second layer of the semicoherent interface, and the Mn-Mn interaction plays an important role in their distribution. Zr atoms mostly segregate on one of the two nonequivalent sites of the second layer of the coherent interface. Due to symmetry properties of the coherent interface, the calculations show that the segregation Zr of atoms to this interface will likely lead to the formation of $L1_2$ ordered Al_3Zr layer.

DOI: 10.1103/PhysRevMaterials.4.073801

I. INTRODUCTION

One of the fundamental challenges for structural materials is to identify alloys that retain favorable mechanical properties at high temperatures. While the required mechanical properties and operation temperature may depend upon both application and the alloy system, a useful metric is the homologous temperature, defined as the temperature divided by the absolute melting temperature, $T_{\text{homog}} = T/T_{\text{melt}}$. Many alloys lose a significant fraction of strength above $T/T_{\text{melt}} > 0.5$. Automotive engines, commonly used alloys based on the Al-Cu system are commonly limited to an upper temperature of 200 °C–250 °C, roughly corresponding to this guideline [1–3]. For this system, Al_2Cu θ' precipitates provide the necessary strength; however, at higher temperatures, these typically rapidly coarsen and transform into the thermodynamically stable θ phase, which fails to strengthen the matrix phase significantly [4–7].

Recent work [8] has demonstrated cast Al-Cu alloys which retain their strength up to temperatures of 350 °C (∼65% of the absolute melting point), through the control of other solute compositions, and whose Al_2Cu θ' precipitates remain stable after 200 hours at this temperature. These alloys are referred to as "ACMZ" alloys, due to the importance of Mn and Zr additions to the Al-Cu system. The levels of Mn and Zr are 0.2 wt. % and Si are 0.01–0.04 wt. %, respectively. Moreover, the amount of Si in the alloy must be controlled; while some is typically added for castability, Ref. [8] suggests <0.1 wt. % is a good choice. The ACMZ alloys studied in [8] have Si levels of 0.03 wt. % or less. The observed microstructure stability is attributed to the segregation of Mn and Zr to the interfaces of the θ' precipitates, observed using atom probe tomography (APT). This segregation presumably both reduces the interfacial energy (and therefore the driving force for the coarsening), and potentially hinders the diffusion of solute atoms as well. Similarly, Si is also observed to segregate to the boundaries. This suggests that Si may compete or otherwise interfere with the segregation of Mn and/or Zr to the interfaces.

Shin *et al.* [9] examined the segregation energetics of a number of potential solutes to the matrix/θ' interfaces. In that work, the energies of isolated solute atoms were calculated at different positions in the matrix and interfaces. The θ' precipitates have a platelike microstructure, with a large fraction of the interface area being associated with a low-energy coherent matrix/θ' interface forming on $\{100\}_{\text{Al}}$ planes, and a higher-energy semicoherent interfaces formed normal to these. The characteristic aspect ratio of the precipitates are commonly

*samolyukgd@ornl.gov
†morrisj@ameslab.gov

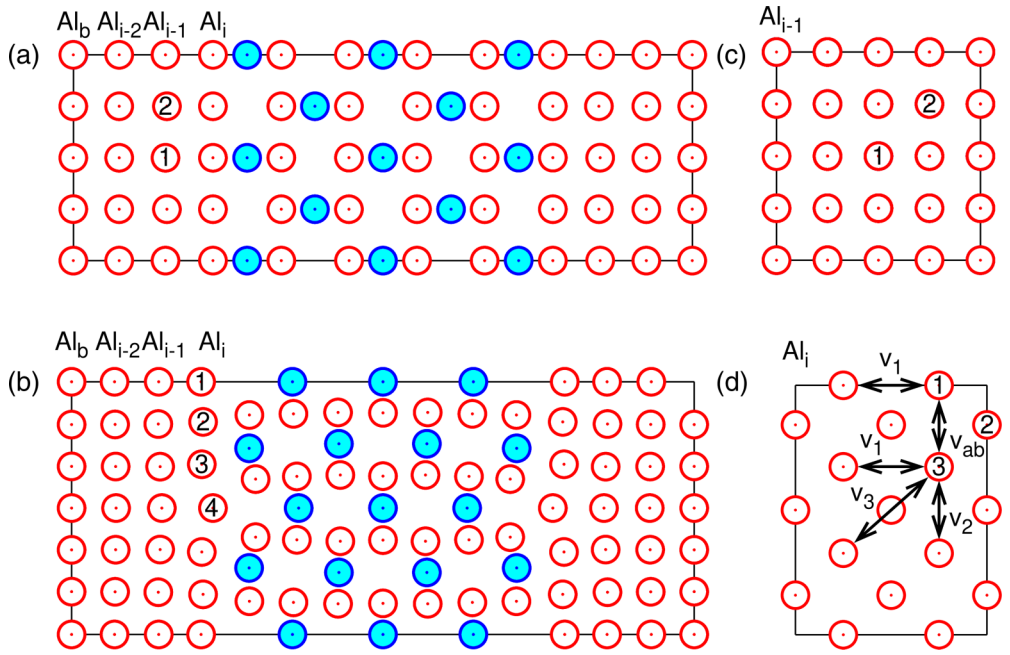

FIG. 1. Supercell used to model (a) coherent and (b) semicoherent interfaces, respectively, after Biswas *et al.* [21]. The semicoherent substitute atoms interactions are shown by arrows in the cross section (d). Here the same notation v_1 is used for two different interaction. However, these two interaction easily can be distinguished, since, in the text, v_1 is always followed by lattice site type (either 1 or 3).

20–100 [10–16]. Atomistic models of these structures are shown in Fig. 1. Shin *et al.* [9] demonstrated that both Mn and Zr show strong tendencies to segregate to both types of interfaces, with Mn favoring the semicoherent interface, and Zr favoring the coherent interface. In addition, Si also has a strong tendency to segregate to the semicoherent interface. These trends are qualitatively consistent with APT measurements shown in Ref. [8].

The goal of this paper is to examine the composition- and temperature-dependent segregation of Mn, Zr and Si to the θ' precipitate interfaces, using a combination of first-principles calculations and statistical mechanical treatments of competing interactions of the different solute atoms, and to compare this with key experimental observations. This goes beyond the work of Ref. [9], in several ways: (1) we consider finite-temperature effects and (2) we consider solute-solute interactions. The latter in particular prevents the application of Langmuir [17] or McClean [18] treatments of interfacial segregation. Moreover, there is a fundamental challenge, that we have not previously seen addressed: for a fixed alloy composition, the matrix/interface compositions are dependent on the total interfacial area. Essentially, this is a problem of constant-composition rather than constant-chemical potential. When the solutes do not interact with each other (the "ideal" case), or when the amount of interface is sufficiently small that the composition of the matrix is essentially fixed independent of interfacial adsorption, this is straightforward. However, neither of this is true for the present case: for the ACMZ alloys, the low solubility of both Mn and Zr results in a large Mn and Zr solute concentration near θ' interfaces, as demonstrated in the APT results [8].

In general, there has not been a clearly developed methodology for calculating concentrations of interfacial concentrations, in the presence of strong material inhomogeneities and with multiple types of interacting solutes. The present work develops and demonstrates such a methodology. In the work below, we develop the methodology, and demonstrate the importance of solute-solute interactions for equilibrium segregation. The results demonstrate two solute-solute interactions consistent with prior experimental work [8]: (i) there is a competition for Mn and Si segregation to the θ' semicoherent precipitate interface, and (ii) Zr-Zr interactions near the θ' precipitate coherent interface reduces the Zr adsorption, but leads to patterning that helps nucleate the Al_3Zr $L1_2$ phase. The calculated equilibrium segregations are important for understanding kinetic effects, including (i) the change in interfacial energies that drive kinetic coarsening and eventually transformation of the precipitate, and (ii) the nucleation and growth of the Al_3Zr $L1_2$ phase near the coherent interface.

The paper is organized as follows. It starts from the presentation of the theoretical approaches and detail of calculation II, which includes developing the relationship between a number of possible substitute atom positions and the volume fraction, size and aspect ratio of the θ' precipitate in the matrix alloy of specified composition in Sec. II A. This also provides the critical concentration of solute atoms fully accommodated by the interface. The expressions for the equilibrium distribution of solute atoms for the basic case of a nonuniform multiphase alloy based on a statistical mechanic formalism is presented in Sec. II B. Section II C addresses the calculation of solute atom energetics including solute-solute interaction. (details of first-principles calculations could be found in Ref. [22]). In Sec. III, we apply the developed formalism to the case of Si, Mn and Zr solute. For the semicoherent interface, we see a complex temperature- and composition-dependent competition between Si and Mn segregation at the semicoherent interface. For Zr on its preferred coherent interface, the Zr-Zr interactions lead to a pattern of segregation that

provides a natural formation of the Al_3Zr $L1_2$ phase. This phase has recently been observed to form on the coherent θ' precipitate [19], and also has been seen for Al_3Sc in high-temperature creep-resistant Al-Cu-Sc [20] alloys. Section IV provides a more detailed summary and discussion relevant to experimental observations.

II. THEORETICAL APPROACHES

In this section the used theoretical approaches are briefly introduced. The reader is addressed to the Ref. [22] for the details. We begin with geometric considerations, both with regards to the atomic structure of the matrix/θ' interfaces, and with regards to the assumptions about the total interfacial area, which is important for the equilibrium segregation. We then present the statistical mechanic approach for self-consistent, mean-field calculations that incorporates the structural inhomogeneity, the total amount of each interface type, and including the solute-solute interactions amongst the different solute types. We present the approach used for calculating solute-solute interactions using density-functional calculations. Finally, we present the compositions associated with a number of Al-Cu alloys of interest.

A. Geometric relations

The system under consideration contains an Al matrix ordered in a face centered cubic (fcc) structure and θ' precipitates in the following composition:

$$(\text{precipitate})_x(\text{matrix}_{1-y-z}\text{A}_y\text{B}_z\text{C}_k)_{1-x}, \tag{1}$$

where x is the fraction of atoms in precipitates, y, z and k are concentrations of impurities of types A, B, and C in the matrix. In the presented approach, it is assumed that the impurity atoms substitute the Al matrix atoms. All possible impurity positions are joined into four groups, i.e., three layers (i, $i-1$ and $i-2$) next to the precipitate and the bulk (b) matrix. A set of relations between the number of possible impurity positions in these groups and alloy composition should be satisfied (see Ref. [22]). In current work, the precipitates are approximated by rectangular prism with squares with side of size R in the base and the top and thickness D measured in the fcc Al lattice parameters.

The supercell used to model θ' precipitate interfaces is shown in Figs. 1(a) for coherent and 1(b) for semicoherent one, respectively. All fcc matrix positions in the first and third layer of the coherent interface, denoted as Al_i and Al_{i-2} in Fig. 1(a), are equivalent.

After some manipulation the relations connecting the local impurity concentration with the alloy composition, $(\text{precipitate})_x(\text{matrix}_{1-y-z}\text{A}_y\text{B}_z)_{1-x}$, can be obtained (see Ref. [22]). Thus the total number of Al atoms in the matrix $N[\text{Al}]$ is

$$N[\text{Al}] = 4N^3(1-x) - \sum_{\alpha} N_{\text{imp}}[\alpha], \tag{2}$$

where $N_{\text{imp}}[\alpha]$ is the number of impurity atoms of type $\alpha \in \{\text{A}, \text{B}\}$, N^3 is the total number of primitive cubic cells with fcc lattice parameter size in the sample. If two possible interfaces (coherent or the semicoherent) are specified by the index β, the number of impurity atoms of type α is

$$N_{\text{imp}}[\alpha] = \sum_{\beta,k,l} N^{\beta}_{i-k,l}[\alpha]c^{\beta}_{i-k,l}[\alpha] + N_b[\alpha]c_b[\alpha], \tag{3}$$

where l is used to specify particular inequivalent atomic positions in the layer $i-k$ with index $k = 0, 1, 2$; $N^{\beta}_{i-k,l}[\alpha]$ and $c^{\beta}_{i-k,l}[\alpha]$ are number of possible substitute α atom positions and their local concentration in these positions, respectively; while, $N_b[\alpha]$ and $c_b[\alpha]$ are the same variables for the "bulk."

TABLE I. Critical substitution atom concentration, y^*, expression for different defect positions at the interface and its numerical value calculated for typical precipitate characteristics presented in the text.

β	position	y^*	value
coherent	$\{i, 1\}, \{i-2, 1\}$	$\frac{1}{D}\frac{x}{1-x}$	0.018
	$\{i-1, l\}$	$\frac{1}{2D}\frac{x}{1-x}$	0.009
semicoherent	$\{i-k, l\}$	$\frac{2}{3R}\frac{x}{1-x}$	0.00029

For an alloy with composition $(\text{precipitate})_x(\text{matrix}_{1-y-z}\text{A}_y\text{B}_z)_{1-x}$ the relations between the number of alloy components and the composition are

$$\begin{aligned} N_{\text{imp}}[\text{A}]/N[\text{Al}] &= y/(1-y-z), \\ N_{\text{imp}}[\text{B}]/N[\text{Al}] &= z/(1-y-z), \\ (N[\text{Al}] + N_{\text{imp}})/(4N^3) &= 1-x. \end{aligned} \tag{4}$$

Obviously, at zero temperature, substitutional solute atoms occupy all available sites of the same type with the lowest defect formation energy. Below, the critical concentrations $y = y^*$ of the substitution atoms which can be completely accommodated by the particular type of the sites are summarized in Table I. For simplicity, it is supposed that there is only one type of substitution atoms. Here, the typical values of the precipitate size are assumed to be $D = 10$ and $R = 400$ (in units of Al lattice parameter), and $x = 0.07$ has been used. Thus, for a solute concentration y larger than 0.018, all $\{i, 0\}$ or $\{i-2, 0\}$ sites (see Table I) at the coherent interface are occupied at zero temperature, and excess solute atoms occupy the alternative sites closest in formation energy. The y^* value is half as large for positions $\{i-1, l\}$, because all positions in this layer of the coherent interface in the layer $i-1$ are split into two groups. Because the thickness of typical precipitates, D, is significantly smaller than width R (typical aspect ratios observed experimentally are $R/D \sim 10$ to 400), the critical concentration, y^*, for semicoherent interface is more than order of magnitude smaller than the coherent interface value. As a result, the semicoherent interface can accommodate approximately 40 times fewer solute atoms.

Solute segregation to the interface has the effect of reducing the interfacial energy, for cases where the segregation is energetically favorable. This affects the driving force for precipitate coarsening. The quantitative estimation of the effect for case of Zr segregation will be presented in Sec. III B. To calculate the effect on the interfacial free energy requires a calculation of the change in free energy with respect to interfacial area, holding other conditions constant. In the coarsening

stage, the total volume of Cu in A_2Cu remains the same. Thus the total volume of all Al_2Cu precipitates is independent of the size of individual precipitates. Since the total precipitate volume is constant, a reduction of the individual precipitate volume is followed by an increase the total precipitates number. The latter results in increase of the total surface area of precipitates [22] and as a result increases the total free energy. As discussed in Sec. III B, while Zr segregation to the coherent interface reduces the interfacial free energy, the interfacial free energy remains positive, and will drive the system towards fewer, larger volume precipitates.

B. The statistical mechanic approach to equilibrium impurity distribution in nonuniform system

As was discussed in previous publications [23–26], the equilibrium defect concentration in nonuniform system can be determined using standard approach. It is adopted to the case of Al-Cu alloy and summarized in Ref. [22]. While this approach incorporates the modification of the system after original single atom substitution by the impurity "exactly," it doesn't contain interactions between impurity atoms. Consequently, it is applicable to the case of low impurity concentration only. By "exactly" we meant that it incorporates energy modification by both electronic structure change and lattice relaxation caused by original atom substitution. A more convenient way to incorporate impurity interactions is to start from the Hamiltonian describing the system with impurities and further use standard statistical mechanic approach [27,28]. Traditionally (Ref. [28] and references therein), this approach is applied to n-component alloys. Below, it will be applied to the case of defects as basic components. For the convenience of the reader, the main expression of the formalism are presented. Consider a system with substitutional impurities of m types, $\alpha = \alpha_1, \alpha_2, \ldots, \alpha_m$. The distribution of impurities over lattice sites is characterized by set of occupancies $\{\hat{n}_{\xi,\alpha}\}$, where $\hat{n}_{\xi,\alpha} = 1$ if the ξth site is occupied by an atom of type α and $\hat{n}_{\xi,\alpha} = 0$ if otherwise. At all ξ operator $\hat{n}_{\xi,\alpha}$ satisfy the condition $\sum_\alpha \hat{n}_{\xi,\alpha} = 1$, so that only $m-1$ of them are independent.

We now consider the case where solute atoms have significant interactions between each other. A general expression for the configurational Hamiltonian $\hat{H}'$ in terms of occupancies $\hat{n}_{\xi,\alpha}$ is

$$\hat{H}' = \sum_\xi \sum_\alpha (\varepsilon_\xi[\alpha] + \psi_{\xi,\alpha})\hat{n}_{\xi,\alpha} + \frac{1}{2}\sum_{\xi\neq\xi'}\sum_{\alpha,\alpha'} V_{\xi,\alpha;\xi'\alpha'}\hat{n}_{\xi,\alpha}\hat{n}_{\xi',\alpha'}, \tag{5}$$

where $\varepsilon_\xi^\beta[\alpha]$ is the change in energy after substituting an Al atom with a solute atom of type α at position ξ, index ξ characterizes the impurity atom position and combine indices β, $i-k$ or b and l, $V_{\xi,\alpha;\xi'\alpha'}$ are the interactions between impurities, and $\psi_{\xi,\alpha}$ is the external field introduced for convenience. In calculations of equilibrium concentrations, one should calculate the thermodynamic potential as a function of temperature and relative chemical potential $\mu_\alpha - \mu_{\mathrm{Al}}$:

$$\begin{aligned} \Omega &= -T \ln \mathrm{Tr} \exp(-\hat{H}/T), \\ \hat{H} &= \hat{H}' - \sum_\xi \sum_\alpha (\mu_\alpha - \mu_{\mathrm{Al}})\hat{n}_{\xi,\alpha}, \end{aligned} \tag{6}$$

where Tr denotes summation over all possible configurations $\{\hat{n}_{\xi,\alpha}\}$. For brevity, the effective Hamiltonian $\hat{H}$ of the grand canonical distribution in Eq. (6) will be referred to as the Hamiltonian. The equilibrium impurity concentration, $c_{\xi,\alpha} = \langle\hat{n}_{\xi,\alpha}\rangle$ is calculated from variation of thermodynamic potential over external field

$$c_{\xi,\alpha} = \frac{\delta\Omega}{\delta\psi_{\xi,\alpha}}, \tag{7}$$

in the limit that the external field $\psi_{\xi,\alpha} \to 0$. Even as the relation (7) formally allows the calculation of the equilibrium impurity concentration at fixed values of temperature and chemical potentials, the actual solution of this system of equation in the case of interacting impurities is a nontrivial problem. Below, the mean-field approximation [29] (MFA) is applied to solve a system of equations (7) (see Ref. [22]).

Using the MFA Hamiltonian and relation (7) it has been obtained that concentration is defined by series of defect formation energies

$$\Delta E_\xi[\alpha] = \varepsilon_\xi[\alpha] - (\mu_\alpha - \mu_{\mathrm{Al}}) \tag{8}$$

modified by defect-defect interaction, where $\varepsilon_\xi[\alpha]$ is the change in energy after substituting an Al atom with a solute atom, and $\mu_\alpha - \mu_{\mathrm{Al}}$ is relative chemical potential.

The system of nonlinear equations (7) should be solved at fixed chemical potential and temperature. In experimental situations, the number of atoms is prescribed rather than the chemical potential, so we used the additional relationships, Eq. (4), to determine the chemical potentials and corresponding defects concentration. These relations preserve the total number of particles [27].

C. Density functional calculations of solute atom energetics

DFT based calculations have been executed using a plane-wave basis set and projector augmented wave [30,31] (PAW) pseudopotential, as implemented in the Vienna *ab initio* simulation package [32,33] (VASP). The detail of the calculation can be found in Ref. [22]. Naturally, the energies $\varepsilon_\xi[\alpha]$ in the Hamiltonian (5) are obtained from the DFT results as follow

$$\varepsilon_\xi[\alpha] = E_\xi[\alpha] - E_\beta, \tag{9}$$

where $E_\xi[\alpha]$ is energy of the interface of type β with atom of type α in position $i-k$ or b and l (the detailed indexes description can be found in Ref. [22]), and E_β is energy of type β interface without impurity. The interaction $V_{\xi,\alpha;\xi'\alpha'}$ is obtained from the DFT energy of the system, $E_{\xi,\alpha;\xi'\alpha'}$, with two impurity atoms α and α' in the positions ξ and ξ' as follows:

$$V_{\xi,\alpha;\xi'\alpha'} = E_{\xi,\alpha;\xi'\alpha'} - E_\xi[\alpha] - E_{\xi'}[\alpha'] + E_\beta. \tag{10}$$

D. Typical cast aluminum alloys

In Table II, we summarize the compositions of typical cast aluminum alloys in order to specify Mn, Zr, and Si atomic concentration of interest. The data from Table 1 in Ref. [8] have been used as an input and rewritten in form (1). Since, in the present research, the distribution of Mn, Zr, and Si is of main interest, other alloying elements are neglected, i.e. it has been supposed that these elements corresponds

TABLE II. Summary of cast aluminum alloy composition Table formula (Precipitate)$_x$(Matrix$_{100-y-z-k}$A$_y$B$_z$C$_k$)$_{100-x}$, with concentration in atomic percent (see text for details). Adapted from Ref. [8]. The alloy names here are conventional, and do not fully reflect the chemical compositions. We indicate the names following Ref. [8] to make specific contact with their notation and the compositions indicated in their Table 1.

Alloy name	Common name	x (precipitate)	y (Si)	z (Mn)	k (Zr)
Al5Cu	–	6.8	0.05	0.0	0.0
Al5CuMg	206	6.8	0.15	0.14	0.0
Al7CuZr	–	8.3	0.05	0.0	0.04
Al7CuMn	–	8.3	0.05	0.11	0.003
Al5CuNiMnZr (ACMZ)	RR350	6.7	0.03	0.11	0.06
Al7CuMnZr (ACMZ)	–	8.5	0.01	0.11	0.04

to Al. Thus the alloy composition is described by formula (precipitate)$_x$(matrix$_{100-y-z-k}$A$_y$B$_z$C$_k$)$_{100-x}$, where x, y, z, and k are at. % of Mn, Si, and Zr, respectively. We would like to emphasize, that starting from this place in the text the concentration is measured in at. %.

III. RESULTS

A. Silicon and manganese solute atoms distribution

As was demonstrated in Shin *et al.* [9], both Si and Mn atoms preferably occupy the Al/θ' semicoherent interface. Thus these two substitute elements are considered in current work simultaneously. To analyze the effect of Si presence on the Mn atoms distribution, the alloy with largest Si concentration, Al5CuMg (206) (Table II), is discussed. The Hamiltonian parameters $\Delta E^{\beta}_{i-k,l}[\alpha] = \varepsilon^{\beta}_{i-k,l}[\alpha] - (\mu_{\alpha} - \mu_{\mathrm{Al}})$ and $V_{(i-k,l),\alpha;(i'-k',l'),\alpha'}$ are summarized in the Tables III and IV. For the solute segregation to the bulk, the index $i-k,l$ is substituted by b. The initial values of these formation energies are obtained using chemical potentials equal to the DFT energy of bulk Si, Mn, and Al per atom, given in Ref. [22]. The chemical potentials μ_{Si}, μ_{Mn} and μ_{Al} in the Eq. (8) for ΔE (presented in the table) are obtained by solving the system of equations (4) at 300 K. Due to the limited size of the modeling supercells, the substitutional atom defect formation energies in the bulk, i.e., at the layer Al$_{\mathrm{b}}$ in Fig. 1, ΔE^{β}_{b}[Si/Mn], calculated separately for the coherent (c) and semicoherent (sc) interfaces shown in the figure, are different from each other. For sufficiently large supercells, we would expect the formation energies in the bulk to be identical for both interfaces. To resolve this issue, below, the $\Delta E^{\beta}_{i-k,l}[\alpha]$ values obtained in the semicoherent interface are shifted by the difference ΔE^{c}_{b}[Si] − ΔE^{sc}_{b}[Si]. This procedure allows us to calculate the Si/Mn atoms concentration in both interfaces simultaneously. From the presented noninteracting defect formation energies, it can be concluded that most Si and Mn solute atoms will be localized at the semicoherent interface. Because of the difference in formation energies, ΔE, of defects in position $\{i, 3\}$ [Fig. 1(b)] and the closest in energy defect in position $\{i, 1\}$ (see Table III) it is expected that almost all $\{i, 1\}$ position will be occupied by Si atoms. In the case of Mn, the substitute atoms will preferably occupy $\{i-1, 1\}$, $\{i, 3\}$, and $\{i, 1\}$ sites.

The calculated solute concentrations at different positions in the interfaces as a function of temperature are presented in Fig. 2, where $x = 7\%$, Si solute concentration $y = 0.15\%$, and Mn concentration $z = 0.15\%$ have been used (the composition of the sample is described by the following formula (precipitate)$_x$(matrix$_{100-y-z}$A$_y$B$_z$)$_{1-x}$). Because the solute concentration of both Si and Mn is much larger than the critical concentration, 0.03%, defined for the semicoherent interface (Table I), there is enough substitute atoms to occupy all available sites at sc interface and their local concentration can reach value 1. In agreement with initial estimate, when solute interactions are neglected, the Si atoms [Figs. 2(b) and 2(c)] occupy predominantly the $\{i, 1\}$ sites. However, the presence of Mn substitute atoms results in significant reduction of Si occupation (about 5%) of this site, while the rest is occupied by Mn. Similarly all Si substitute atoms are expelled from the $\{i, 3\}$ position at the semicoherent interface by Mn atoms. The local concentration of Mn substitute in sites $\{i, 3\}$ and$\{i-1, 1\}$ is close to 1 at room temperature.

With such significant Si and Mn concentrations at the layer i and $i-1$ of the semicoherent interface, the interaction between substitute atoms can't be neglected. The results for the Si and Mn atoms interaction obtained using Eq. (10) are summarized in Table IV. These interactions are incorporated into the system of equations presented in Ref. [22].

The first obvious modification of the solute concentration after introduction of interaction is the change of Mn atoms concentration from fully occupied in sites $\{i, 3\}$ [shown by empty light brown color pentagon shaped dots in Fig. 2(e)]

TABLE III. The noninteracting Si/Mn defect formation energies ΔE in different position at the interfaces and in the bulk, in eV. The chemical potentials μ_{Si}, μ_{Mn}, and μ_{Al} in the Eq. (8) for ΔE are obtained by solving system of equations (4) at 300 K. Notations c or sc identify coherent or semicoherent interfaces (index β).

	c_{i-2}	$c^{(1)}_{i-1}$	$c^{(2)}_{i-1}$	c_i	c_b	$sc^{(4)}_{i-2}$	$sc^{(3)}_{i-1}$	$sc^{(1)}_{i-1}$	$sc^{(3)}_{i}$	$sc^{(2)}_{i}$	$sc^{(1)}_{i}$
Mn	0.34	0.15	0.08	0.63	0.18	0.20	—	−0.26	−0.27	0.31	−0.12
Si	0.20	0.26	0.25	0.23	0.17	0.16	0.17	—	0.02	0.14	−0.09

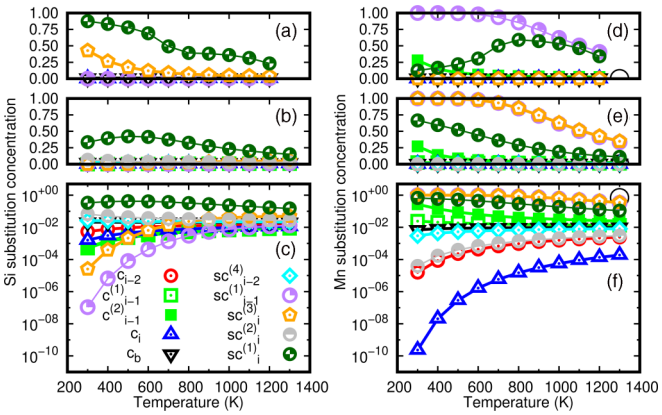

FIG. 2. Interfacial solute compositions in alloy $(\text{precipitate})_x(\text{matrix}_{100-y-z}\text{Si}_y\text{Mn}_z)_{1-x}$, where $y = 0.15$ at. % and $z = 0.15$ at. %, corresponding to the content for an Al 206 alloy. (a) Calculated local Si atom concentration (at. %) obtained with incorporated interaction [Fig. 1(d) and Table IV] presented with linear y-axis scale. (b) Calculated local Si atom concentration with linear y-axis scale, obtained by neglecting the interaction between substitution atoms; (c) the same with logarithmic y-axis scale. [(d)–(f)] Similar results for Mn substitute with interacting solute atoms (d) and with noninteracting [(f) and (e)], respectively.

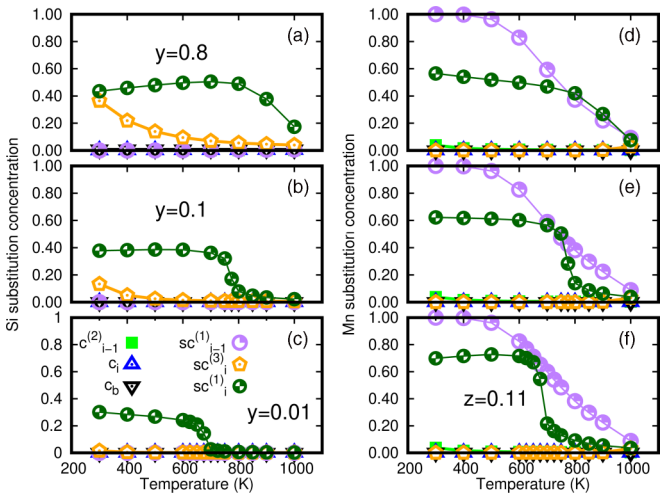

FIG. 3. Equilibrium Si [(a)–(c)] and Mn [(d)–(f)] atoms distribution at semicoherent interface in alloy $(\text{precipitate})_x$ $(\text{matrix}_{100-y-z}\text{Si}_y\text{Mn}_z)_{1-x}$, where $x = 7\%$, $z = 0.11\%$, and [(a) and (d)] $y = 0.8\%$, [(b) and (e)] 0.1%, and [(c) and (f)] 0.01%.

to practically empty [Fig. 2(d)]. This happened because of the introduction of the strong repulsion, 0.206 eV (Table IV), between Mn atoms occupying sites $\{i, 3\}$. Instead, these freed $\{i, 3\}$ sites become occupied by Si solute; this may be seen by the increased occupancy in Fig. 2(a) compared with that of Fig. 2(b). However, these sites can not be fully occupied by Si atoms even at zero temperature, because of the effective repulsion obtained as a sum of interactions V_1, V_2, and V_3 (last line in Table IV) multiplied by number of the neighbors. In the MFA approach the interactions are incorporated as an effective ones. Thus even at zero temperature only 25% of $\{i, 3\}$ sites are occupied by Si. An additional factor significantly reducing the presence of Mn atoms in the site $\{i, 3\}$ is the strong repulsion, 0.407 eV, between Mn occupying $\{i-1, 1\}$ and $\{i, 3\}$ sites. Consequently, Mn substitute predominantly occupy sites $\{i-1, i\}$ shown by purple color partially filled circles in Fig. 2(d). The interaction between Mn in $\{i-1, i\}$ position, −0.002 eV, is negligibly small, and its incorporation doesn't significantly change the concentration of solute atoms.

One of the strongest interactions between solute atoms corresponds to the −0.230 eV attraction between Mn and Si atoms occupying $\{i, 1\}$ sites. It results in redistribution of Mn/Si atoms between these sites, and changes the character of concentration temperature dependence show by green color half-filled points in Fig. 2. Thus, before incorporating interaction at low temperature, 5% [Fig. 2(b)] of $\{i, 1\}$ sites were occupied by Si, while the rest by Mn [Fig. 2(e)]. After turning on interactions, the sites are occupied by Si by almost 35% [Figs. 2(a) and 2(d)]. Also, the shape of temperature dependence has been changed. A fast drop of Mn concentration with the temperature (Fig. 2) is changed to a almost constant dependence up to 800 K followed by sharp reduction above this temperature.

In order to illustrate the effect of Si presence on Mn precipitation at the semicoherent interface, we calculated equilibrium Mn/Si local atomic concentrations in a series of alloys with Si concentration changing from $y = 0.01\%$ to 0.8% and constant Mn concentration. The Mn concentration was chosen to be 0.11 at. %, typical for ACMZ alloy (Table II). The result for three Si concentration are presented in Fig. 3. The increase of Si concentration results in rising presence of Si substitute atoms in $\{i, 1\}$ site of semicoherent interface and as a result reduction of Mn substitute concentration at this site by $\approx 15\%$. It, also, significantly increases presence of Si atoms in $\{i, 3\}$ sites. Si presence in these sites changes from negligibly small value at $y = 0.01\%$ to 40% at $y = 0.8\%$.

Figure 3 demonstrates that the local concentration of Si/Mn atoms at $\{i, 1\}$ sites changes sharply with temperature, suggesting a phase transition (green circles). The temperature of this sharp local concentration change increases with increasing Si concentration, y. This change occurs at 670 and 770 K, at Si concentrations of $y = 0.01$ and 0.1, respectively.

TABLE IV. The interaction defined in the Hamiltonian (8) between Si and Mn atoms in the semicoherent interface occupying $\{i, 1\}$, $\{i, 3\}$, and $\{i-1, 1\}$ sites. See notation in Fig. 1(d). V_{ab} interaction for Si atom occupying $\{i, 1\}$ and $\{i, 3\}$ sites separated by nearest neighbors distance is shown in Fig. 1(d). V_{ab} Mn-Mn interactions corresponds two Mn substitute placed in $\{i, 1\}$ and $\{i-1, 1\}$ sites and separated by nearest neighbors distance (is not shown in the Fig. 1). V_{Si-Mn} describes interaction of Si and Mn substitute occupying $\{i, 1\}$ sites and separated by nearest neighbors distance. All values are in eV.

atom	position	V_{ab}	V_1	V_2	V_3	$V_{\text{Si-Mn}}$
	$\{i-1, 1\}$	0.407	−0.002			
Mn	$\{i, 3\}$	0.407	0.206			
	$\{i, 1\}$		−0.069			−0.230
	$\{i, 1\}$	0.009	−0.004			−0.230
Si	$\{i, 3\}$	0.009	−0.095	0.045	0.047	

TABLE V. The noninteracting Zr defect formation energies, ΔE, in different position at the interfaces and in the bulk, in eV. The chemical potentials $\mu_{\rm Zr}$ and $\mu_{\rm Al}$ in the Eq. (8) for ΔE are obtained by solving system of equations (4) at 300 K. The notation c or sc identify coherent or semicoherent interfaces (index β).

	c_{i-2}	$c^{(1)}_{i-1}$	$c^{(2)}_{i-1}$	c_i	c_b	$sc^{(4)}_{i-2}$	$sc^{(2)}_{i-1}$	$sc^{(1)}_{i-1}$	$sc^{(3)}_i$
Zr	1.26	−0.19	0.1	0.23	0.64	0.87	0.86	0.54	0.40

At $y = 0.8$, this sharp change is suppressed completely. Interestingly, this indicates that at high temperatures, reducing the Si composition has the effect of reducing Mn concentration at this site. Presumably, this is due to the strong attractive interaction between Si and Mn for this site (see Table IV). Atom probe tomography studies [8] indicate that Si and Mn compete to affect the thermal stability of θ' precipitates in ACMZ alloys.

B. Zirconium substitution distribution

Below, we discuss results for Zr, particularly examining concentrations $y = 0.8$ at. % in alloy with composition described by formula $(\text{precipitate})_x(\text{matrix}_{100-y}\text{Zr}_y)_{100-x}$ relevant for the ACMZ alloys. The Hamiltonian parameters $\Delta E^{\beta}_{i-k,l}[\alpha] = \varepsilon^{\beta}_{i-k,l}[\alpha] - (\mu_\alpha - \mu_{\rm Al})$ and $V_{(i-k,l),\alpha;(i'-k',l'),\alpha'}$ for the case of Zr are presented in the Tables V and VI. Similar to the case of Si and Mn, the initial values of these formation energies are obtained using of chemical potentials equal to the DFT energy of bulk Zr and Al per atom, given in Ref. [22].

From the result in Table V it can be concluded that at zero temperature Zr atoms will predominantly occupy the coherent interface. This result is consistent with the experimentally observed low solubility of Zr. We note that Zr has slow diffusion in bulk Al, and therefore experimentally observed concentrations in cast alloys may not represent equilibrium values. The Zr-Zr interactions are summarized the Table VI.

The results for the temperature-dependent Zr solute atom distribution are presented in Fig. 4. Zr atoms are segregated on the first two layers of the coherent interface. Due to symmetry properties of the coherent interface, all positions in layers i and $i-2$ are equivalent, while layer $i-1$ has two nonequivalent sites. The sites $\{i-1, 1\}$ are placed in the same column, oriented perpendicular to the interface, with Cu atoms in θ' precipitate. Of these two nonequivalent sites, the site $\{i-1, 1\}$ is almost fully occupied up to 800 K. Above this temperature the concentration of noninteracting Zr atoms, $c^{(1)}_{i-1}$ starts to decrease [Figs. 4(a) and 4(b)] and some of the Zr atoms redistribute between the $\{i-1, 2\}$ sites and sites of layer i of the interface.

TABLE VI. The interaction defined in the Hamiltonian (8) between Zr atoms in the coherent interface in position $\{i-1, 1\}$ and $\{i-1, 2\}$. V_1 corresponds interaction of Zr atoms in the same lattice site $\{i-1, 1\}$ or $\{i-1, 2\}$ separated by an Al conventional lattice parameter (next nearest neighbor interactions), while, V_{ab} are nearest neighbor interactions between Zr in two different sites $\{i-1, 1\}$, $\{i-1, 2\}$. All values are in eV.

atom	position	V_{ab}	V_1
	$\{i-1, 1\}$	0.416	−0.202
Zr	$\{i-1, 2\}$	0.416	−0.272

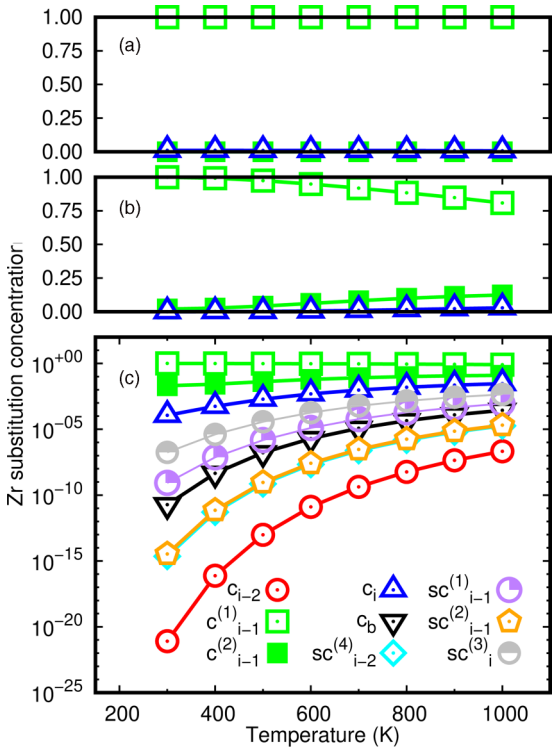

FIG. 4. Equilibrium Zr solute atom distribution: (a) linear y-axis scale obtained by incorporating interactions between Zr atoms; (b) linear y-axis scale, calculated with no interaction between Zr atom; and (c) the same as (b), but logarithmic y-axis scale.

The introduction of Zr-Zr interaction makes the asymmetric character of Zr atoms distribution in the $i-1$ layer even more pronounced, creating a correlation of Zr atoms near the interface that is similar to the ordered $L1_2$ phase that is observed for Al_3Zr. The attractive interaction between Zr atom in $\{i-1, 1\}$ sites makes the effective Zr defect formation energy even lower, creating an alternate Zr occupancy in this layer. The repulsion between Zr atoms occupying $\{i-1, 2\}$ sites forces Zr atoms to leave this sub-lattice. As a result, the $\{i-1, 1\}$ sites are fully occupied by Zr atoms at all temperatures up to 1000 K [Fig. 4(c)] and $\{i-1, 2\}$ sites are almost empty (local concentration is less than 3×10^{-3} at. %). The local concentration of Zr atoms at i sites is slightly increased up to 0.05. This symmetry breaking in first three Al matrix layers next to precipitate results in formation of $L1_2$ (Al_3Zr) structure, i.e. layers i and $i-2$ are predominantly occupied by Al, while half of sites in layer $i-1$ are occupied by Zr and half by Al. The formation of the $L1_2$ phase on the coherent Al/Al_2Cu interface was recently observed experimentally [19], similar to those seen in some Al-Cu-Sc alloys [20].

As was discussed above in Sec. II A, the solute segregation to the interface affects the driving force for precipitate coarsening. The change in interfacial free energy may be calculated

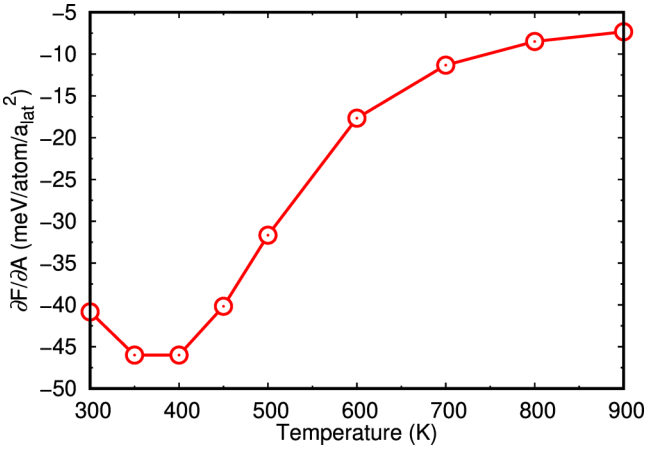

FIG. 5. The derivative of free energy change F due to Zr atoms segregation with precipitates surface area A_{Zr} at different temperatures.

as the change in free energy with respect to the coherent free energy:

$$\Sigma = \frac{\partial F}{\partial A_{\text{coh}}} \tag{11}$$

This has two primary contributions: One of these is the "bare" interfacial energy Σ_0 for the pure Al/Al_2Cu interface. For the coherent interface, the bare interfacial energy has been calculated in the range of $\Sigma_0 = 170$–250 mJ/m^2 [9,21,34]. Typically, entropic effects are ignored for Σ_0, particularly for the highly ordered, coherent interface. We denote the total interfacial free energy as $\Sigma = \Sigma_0 + \Sigma_{Zr}$, where the effects of Zr solute segregation are specifically separated out. Our methodology does not directly address Σ_0, taking the interface as part of the overall structure as described in Sec. II A, and not considering its energy explicitly. However, the effects of Zr on the free energy, and how that changes with an infinitesimal change in interfacial area, may be directly calculated using the above equation. We note that, unlike Σ_0, we anticipate significant entropic effects: a single Zr atom segregating from the Al matrix to the interface has a significant reduction of energy (nearly 0.5 eV [9]), but undergoes a significant loss of configurational entropy. In the dilute limit, where the Zr atoms are dilute on the interface and Zr-Zr interactions may be neglected, the energetic contributions to Σ_{Zr} may be directly estimated using the segregation energy and the areal density of Zr [8]. However, as our calculations above demonstrate, for the alloys considered, the Zr-Zr interaction may be significant, and the concentration of Zr on the coherent interface is significant.

Our approach allows for a direct, small change in area, keeping other aspects fixed, as described in Sec. II A. We have used this, to calculate the free energy required for a small increase in interfacial area, per the equation above. As we consider only the effects of Zr, this directly gives Σ_{Zr}. This has been done numerically by changing the number of precipitates while keeping the total volume fixed, thus increasing the surface area of the precipitates, which is dominated by the coherent interface. Figure 5 illustrates the effect of the derivative of free energy change with respect to the precipitate surface area due to Zr segregation, as a function of temperature. The derivative is negative at all temperatures, thus, the coherent interfacial energy is reduced, thereby reducing the driving force for precipitate coarsening. At relevant temperatures ($\sim$600 K), the reduction is approximately $\Sigma_{Zr} = -20$ mJ/m^2, thus reducing the interfacial free energy by $\sim$10% from Σ_0.

IV. DISCUSSION AND CONCLUSIONS

The equilibrium distribution of solute atoms at interface between fcc Al and θ' Al_2Cu precipitate has been investigated using combination of DFT and mean-field statistical mechanics methods. The approach developed here naturally incorporates the dependence of the distribution not only from the temperature and position of substitute atom in the specific type (coherent or incoherent) of the interface, but also the composition of alloy, volume and aspect ratio of θ' precipitate, and volume fraction of the precipitates. Moreover, the approach incorporates important solute-solute interactions, and demonstrates their importance for alloys based on the Al-Cu system. As an input, we used the DFT-calculated supercell energy change caused by substitution of Al by one solute atom (solute segregation energy) or two atoms (solute-solute interaction). The developed approach incorporates exactly the elastic contribution to energy change associated with Al atom substitution by solutes.

The technique was applied to investigate Si, Zr, and Mn substitute atom segregation at the fcc Al/θ' Al_2Cu precipitate interface, due to their relevance in ACMZ alloys that exhibit high-temperature θ' stability [8].

(1) Competing Si and Mn solute atoms segregate on the same semicoherent interface, and that the presence of Si reduces concentration of Mn substitute at the interface. In addition to thermodynamic equilibrium results, the solute atoms kinetic should be taken in to consideration. Thus Si atoms diffuse in Al is six orders of magnitude faster than compared to Mn at 300 C (see Ref. [8] and the figure with diffusion properties in Ref. [22]). As a result, Si atoms most likely will occupy the semicoherent interface.

(2) Si atoms preferably occupy the first layer of the interface and share one of particular sites in the layer with Mn atoms, reducing Mn atoms present in this layer.

(3) Mn atoms preferably occupy the second layer of semicoherent interface. The strong repulsion between Mn atoms in first and second layer results in removing Mn atoms from one type of the sites in first layer, making space for Si atoms.

(3) Zr atoms predominantly occupy the second layer [$i-1$ in Fig. 1(a)] of the coherent interface. Due to specifics of the coherent interface symmetry, all sites in the layers i and $i-2$ are equivalent, while layer $i-1$ sites has two nonequivalent positions. Only one of these positions are predominantly occupied by Zr atoms. Such a distribution of Zr atoms results in the creation of an $L1_2$ Al_3Zr layer at the coherent interface. Further incorporation of the Zr-Zr interaction only emphasize the $L1_2$ character of Zr distribution: the $\{i-1, 1\}$ sites are fully occupied by Zr at all temperatures up to 1000 K, while the $\{i-1, 2\}$ sites are fully occupied by Al. This finding agrees with experimental observation.

These calculations are directly relevant to the formation of stable θ' precipitates observed in the ACMZ alloys [8]. For

these alloys, the dominant factor appears to be the addition of Mn. However, the level of Si (which is commonly added for castability of Al alloys) must be limited; too much Si appears to reduce the stability. The calculations in Ref. [9] demonstrate that both Mn and Si tend to segregate preferentially to the θ' semicoherent interface, and atom-probe experiments show heightened Si and Mn levels near that interface [8]. The $\theta' \rightarrow \theta$ transformation likely occurs near the high-energy semicoherent interface, and a reasonable conjecture is that Mn segregation to that interface helps prevent the transformation, while Si (which also preferentially segregates to that interface) does not. Here, we demonstrate that this occurs, though the amount of Mn reduction is not large, and that Mn at the interface will be suppressed by the addition of Si. In Fig. 3, for Si concentration 0.01%, the local concentration of Mn in site $sc_{i-1}^{(1)}$ equal 1, and in site $sc_i^{(1)} = 0.8$. For Si $y = 0.8\%$ these local concentrations are 1 and 0.6, respectively. Thus the relative change in accommodation of Mn equal

$$\frac{0.2 \times 2/(3R) \times x/(1-x)}{1 \times 2/(3R) \times x/(1-x) + 0.8 \times 2/(3R) \times x/(1-x)} = 0.2/1.8 \rightarrow 11\%.$$

The ACMZ alloys are further stabilized by the addition of Zr, which preferentially goes to the coherent interface [8]. Here, our calculations indicate that while Zr strongly segregates to this interface, repulsive near neighbor Zr-Zr interactions in the Al matrix (V_{ab} in Table VI) limit the amount that is likely to accumulate. However, next-nearest neighbor interactions are found to be favorable (V_1 in Table VI for the favorable site $\{i-1, 1\}$); thus, at very low concentrations, Zr solute atoms are likely to form "islands" near the θ' precipitates with Zr-occupied next-nearest-neighbor interactions. This pattern of Zr formation on the Al (100) planes is identical to the structure of these planes in the $L1_2$ Al_3Zr, which has a very small misfit relative to the bulk Al lattice. This suggests that the cast alloy, with a super-saturation of Zr in the Al matrix, can preferentially nucleate the Al_3Zr phase on the θ' precipitates, as has been recently observed [19]. We note that this process is similar to that described for Al-Cu-Sc alloys [20], where Al_3Sc precipitates on the θ' phase, and conversely, after resolutionizing the Cu into the Al matrix at high temperatures, the θ' phase forms on the Al_3Sc precipitates, resulting in a microstructure that is creep-resistant at 300 °C.

While the focus of the present paper is on equilibrium distributions, the implications of the results have important kinetic considerations. In the simplest form, the Si, Mn and Zr solutes all energetically favorably tend to segregate to the interfaces. This has two immediate likely effects on precipitate coarsening. First, precipitate coarsening is largely driven by the interfacial free energy. The strong segregation tendencies have the effect of reducing the interfacial free energy. This may be understood simply by noting that (in equilibrium) a reduction of interfacial area will reduce the amount of solute at the interfaces, driving the solute atoms into a higher energy state. Given the strong interaction of the solutes with the interfaces, the interfacial free energy reduction is significant, as discussed in the text. Secondly, the solute segregation is likely to slow the motion of the interfaces under a given driving force, particularly for the slowly diffusing solute atoms Mn and Zr. Thus, there is likely to be a reduction in both the driving force and a kinetic effect that reduces the rate of coarsening. Finally, the Zr-Zr interaction near the coherent interface is demonstrated to provide a natural nucleation site for the Al_3Zr phase. Conversely, it is important to note that kinetic effects are likely to result in deviations in the observed solute segregation. In this paper, we demonstrate that Mn and Si compete in equilibrium for occupancies near the semicoherent interface. However, the faster mobility of Si may result in enhanced segregation to the interface, as it may arrive more quickly, and equilibration may be slow due to the slower motion of Mn, and potentially the need to displace Si that has already arrived. In the case of Zr, the diffusion rates are very small, and observed matrix concentrations are significantly higher than equilibrium.[8] Despite the slow kinetics, experiments show a strong segregation of Zr to the interface. Long aging times at high temperatures will be necessary to reach equilibrium. Nevertheless, our calculations demonstrate the strong tendency of Zr to segregate to the interface, consistent with observations, and the tendency to form the Al_3Zr phase at the interface.

In summary, we present an approach to calculate solute segregation at interfaces, in the presence of multiple solute interactions, and apply this to solutes relevant to the ACMZ alloys [8] that are stable to high homologous temperatures due to the addition of Mn and Zr. We also treat the complication that such segregation depends not only on solute concentration and temperature, but also the θ' precipitate density and morphology. Mn preferentially segregates to the Al/θ' semicoherent interface, but this may be limited due to the competing segregation of Si. Zr preferentially goes to the coherent interface, where Zr-Zr solute interactions can lead to a natural formation of a layer of Al_3Zr located near the interface.

ACKNOWLEDGMENTS

We acknowledge support through the U.S. Department of Energy's Energy Efficiency and Renewable Energy, Vehicle Technologies Office, Powertrain Materials Core Program. Initial results were sponsored by the Laboratory Directed Research and Development Program of Oak Ridge National Laboratory, managed by UT-Battelle, LLC, for the U.S. Department of Energy. This research used resources of the National Energy Research Scientific Computing Center (NERSC), a U.S. Department of Energy Office of Science User Facility operated under Contract No. DE-AC02-05CH11231.

[1] M. Javidani and D. Larouche, Int. Mater. Rev. **59**, 132 (2014).
[2] S. Roy, L. F. Allardi, A. Rodriguez, W. D. Porter, and A. Shyam, Metall. Mater. Trans. A **48**, 2543 (2017).
[3] S. Roy, L. F. Allard, A. Rodriguez, T. R. Watkins, and A. Shyam, Metall. Mater. Trans. A **48**, 2529 (2017).
[4] E. Hornbogen, J. Light Metals **1**, 127 (2001).

[5] A. Wilm, Metallurgie **8**, 223 (1911) [(Translated fo English), J. W. Martin, *Precipitation Hardening* (Pergamon Press, Oxford, 1968), pp. 103–111].
[6] D. A. Porter, K. E. Easterling, and M. Y. Sherif, *Phase Transformations in Metals and Alloys* (Routledge, 2009).
[7] C. Laird and H. Aaronson, Acta Metall. **14**, 171 (1966).
[8] A. Shyam, S. Roy, D. Shin, J. Poplawsky, L. Allard, Y. Yamamoto, J. Morris, B. Mazumder, J. Idrobo, A. Rodriguez, T. Watkins, and J. Haynes, Mater. Sci. Eng. A **765**, 138279 (2019).
[9] D. Shin, A. Shyam, S. Lee, Y. Yamamoto, and J. A. Haynes, Acta Mater. **141**, 327 (2017).
[10] K. Kim, A. Roy, M. Gururajan, C. Wolverton, and P. Voorhees, Acta Mater. **140**, 344 (2017).
[11] H. Liu, B. Bellón, and J. LLorca, Acta Mater. **132**, 611 (2017).
[12] D. Mitlin, J. W. Morris, Jr., and V. Radmilovic, Metall. Mater. Trans. A **31**, 2697 (2000).
[13] P. Merle and J. Merlin, Acta Metall. **29**, 1929 (1981).
[14] P. Merle and F. Fouquet, Acta Metall. **29**, 1919 (1981).
[15] J. Boyd and R. Nicholson, Acta Metall. **19**, 1379 (1971).
[16] J. da Costa Teixeira, L. Bourgeois, C. Sinclair, and C. Hutchinson, Acta Mater. **57**, 6075 (2009).
[17] I. Langmuir, J. Am. Chem. Soc. **40**, 1361 (1918).
[18] D. McLean, *Grain Boundaries in Metals*, Monographs on the Physics and Chemistry of Materials (Oxford, Clarendon Press, 1957).
[19] J. D. Poplawsky, B. K. Milligan, L. F. Allard, D. Shin, P. Shower, M. F. Chisholm, and A. Shyam, Acta Mater. **194**, 577 (2020).
[20] Y. H. Gao, C. Yang, J. Y. Zhang, L. F. Cao, G. Liu, J. Sun, and E. Ma, Mater. Res. Lett. **7**, 18 (2019).
[21] A. Biswas, D. J. Siegel, C. Wolverton, and D. N. Seidman, Acta Mater. **59**, 6187 (2011).
[22] See Supplemental Material at http://link.aps.org/supplemental/10.1103/PhysRevMaterials.4.073801 for important details on the modeling, including the geometry considered for interfacial segregation calculations, details of the statistical mechanical approach, DFT calculations of solute atom energetics, Si/Mn/Zr substitutional energetics and their diffusional behaviors in Al.
[23] G. D. Samolyuk and Y. N. Osetsky, J. Phys.: Condens. Matter **27**, 305001 (2015).
[24] G. D. Samolyuk, B. Ùjfalussy, and G. M. Stocks, J. Appl. Phys. **116**, 173908 (2014).
[25] C. L. Fu, Y.-Y. Ye, M. H. Yoo, and K. M. Ho, Phys. Rev. B **48**, 6712 (1993).
[26] J. Mayer, C. Elsässer, and M. Fähnle, Phys. Status Solidi B **191**, 283 (1995).
[27] L. D. Landau, E. M. Lifsic, L. P. Pitaevskii, J. B. Sykes, and M. J. Kearsley, *Statistical Physics*, Part 1 (Elsevier/Butterworth-Heinemann, Amsterdam, 2009).
[28] V. G. Vaks and G. D. Samolyuk, J. Exp. Theor. Phys. **88**, 89 (1999).
[29] G. F. Newell and E. W. Montroll, Rev. Mod. Phys. **25**, 353 (1953).
[30] P. E. Blöchl, Phys. Rev. B **50**, 17953 (1994).
[31] G. Kresse and J. Furthmüller, Comput. Mater. Sci. **6**, 15 (1996).
[32] G. Kresse and D. Joubert, Phys. Rev. B **59**, 1758 (1999).
[33] G. Kresse and J. Furthmüller, Phys. Rev. B **54**, 11169 (1996).
[34] V. Vaithyanathan, C. Wolverton, and L. Q. Chen, Acta Mater. **52**, 2973 (2004).